



# Mechanistic insights into the iridium-catalyzed hydrosilylation of allyl compounds



Korbinian Riener<sup>a</sup>, Teresa K. Meister<sup>a</sup>, Peter Gigler<sup>b</sup>, Wolfgang A. Herrmann<sup>a</sup>, Fritz E. Kühn<sup>a,\*</sup>

<sup>a</sup> Chair of Inorganic Chemistry/Molecular Catalysis, Catalysis Research Center and Department of Chemistry, Technische Universität München, Lichtenbergstr. 4, 85747 Garching bei München, Germany

<sup>b</sup> Wacker Chemie AG, Consortium für elektrochemische Industrie, Zielstattstraße 20, 81379 München, Germany

## ARTICLE INFO

### Article history:

Received 3 August 2015

Revised 6 September 2015

Accepted 8 September 2015

### Keywords:

Allyl compounds

Deactivation

Hydrosilylation

Iridium catalysis

Mechanism

Silanes

## ABSTRACT

The hydrosilylation of allyl compounds is very important for the industrial production of  $\gamma$ -substituted propylsilanes; however, it is also a process known to suffer from either substantial selectivity issues or short catalyst lifetimes. While there are reports on the platinum-catalyzed variant, this study is the first comprehensive work on the more recently employed iridium-catalyzed process. A combination of stoichiometric and catalytic experiments as well as reactions with isotope-labeled compounds is used to elucidate the critical parameters influencing the catalytic performance and to identify the main deactivation pathways. This report is intended to pave the way toward the optimization of current iridium-catalyzed processes and the design and synthesis of improved catalyst structures.

© 2015 Elsevier Inc. All rights reserved.

## 1. Introduction

The hydrosilylation of C–C multiple bonds is the key catalytic reaction to access organosilicon compounds that are of high industrial importance for the production of organofunctionalized silanes and silicones and are an integral part of polymers, crosslinkers and adhesives [1–3]. Within this field, the hydrosilylation of allyl compounds to yield  $\gamma$ -substituted propylsilanes is of particular interest due to the multiple functionalities of the obtained products. Their efficient synthesis remains one of the current challenges in hydrosilylation catalysis (Scheme 1) [1,2,4].

The common platinum-based hydrosilylation catalysts were employed in these transformations and mechanistic studies have revealed several reaction pathways, in some cases leading to by-product formation and thus low selectivities [4–10]. This holds true especially for the hydrosilylation of allyl chloride, which is the most widely used allyl compound in industry [1,2]. Since these selectivity issues are an intrinsic problem of platinum catalysis, it appears worthwhile to focus on other systems. Iridium catalysis was reported as an efficient tool to overcome the problems concerning selectivity, with the most prominent catalyst precursor being  $[\{\text{IrCl}(\text{COD})\}_2]$  [11–23]. However, these catalyst systems

exhibit short catalyst lifetimes, resulting in low yields and the necessity for high metal loadings, which is the main drawback concerning their economic use [1,2]. The catalyst loadings can be reduced by addition of co-catalysts such as cyclooctadiene (COD), but a detailed mechanistic picture to understand the catalytic system on a molecular level is still missing. To date, patent literature is almost the sole source of information [11–23]. In this work, the first comprehensive mechanistic study on the iridium-catalyzed hydrosilylation of allyl compounds is presented, also revealing the main deactivation pathways. The results from both stoichiometric and catalytic experiments will be helpful to pave the way toward the design and implementation of more efficient catalyst systems.

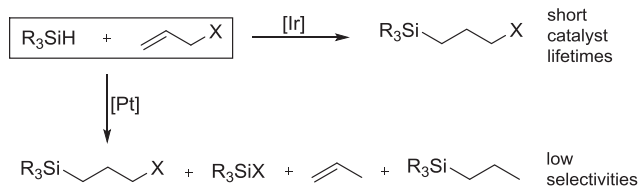
## 2. Experimental methods

### 2.1. General remarks

All reactions were performed in an argon atmosphere using standard Schlenk and glove box techniques. All solvents and reagents were purified, dried and degassed in line with standard purification techniques [24]. Allyl chloride- $d_2$  was synthesized according to a literature procedure [4].  $[\{\text{IrCl}(\text{COD})\}_2]$  was purchased from Sigma Aldrich and used as received. NMR spectra were acquired on a Bruker Avance Ultrashield 400 MHz spectrometer. All

\* Corresponding author. Fax: +49 89 289 13473.

E-mail address: [fritz.kuehn@ch.tum.de](mailto:fritz.kuehn@ch.tum.de) (F.E. Kühn).



**Scheme 1.** Ir- and Pt-catalyzed hydrosilylation of allyl compounds [1,2,4].

$^1\text{H}$  and  $^{13}\text{C}$  chemical shifts are reported in parts per million (ppm) relative to TMS, with the residual solvent peak serving as internal reference [25]. Elemental analyses were performed in the microanalytical laboratory of TUM-CRC and FAB mass spectrometry was carried out using a Finnigan MAT 90. A Jasco VT-550 photometer was used to conduct the UV–Vis measurements in dichloromethane. TEM images were recorded at a nominal magnification of 250,000 on a JEOL JEM 2011 electron microscope operated at 120 kV. The samples were prepared by adding a drop of the iridium nanoparticles suspended in ethanol on copper grids covered with a Quantifoil Multi A holey carbon film and a 2 nm carbon film on top.

## 2.2. Catalytic reactions

### 2.2.1. General protocol for hydrosilylation experiments

A mixture of  $[\{\text{IrCl}(\text{COD})\}_2]$ , cyclooctadiene (COD) and the allyl compound (55.0 mmol, 1.0 equiv.) is stirred (500 rpm) at 40 °C for 10 min in a reaction flask equipped with a reflux condenser. At this temperature, the silane (55.0 mmol, 1.0 equiv.) is added using a Landgraf LA-30 syringe pump, followed by the addition of 1.28 mL mesitylene (1.10 g, 9.15 mmol, 6.0 equiv.) as internal standard. The reaction mixture is further stirred for 10 min at 40 °C and an aliquot is taken for NMR analysis.

### 2.2.2. Hydrosilylation of allyl chloride- $d_2$ and $\text{Me}_2\text{SiHCl}$

In an NMR tube equipped with a J. Young valve, 4.10 mg  $[\{\text{IrCl}(\text{COD})\}_2]$  (6.10  $\mu\text{mol}$ , 14.6 mol% Ir) is dissolved in 0.7 mL  $\text{CD}_2\text{Cl}_2$ . 7.00  $\mu\text{L}$  allyl chloride- $d_2$  (6.58 mg, 83.8  $\mu\text{mol}$ , 1.0 equiv.) is added to the reaction mixture and the NMR tube is shaken for 15 min, followed by addition of 9.20  $\mu\text{L}$   $\text{Me}_2\text{SiHCl}$  (7.91 mg, 83.6  $\mu\text{mol}$ , 1.0 equiv.). Mesitylene is used as internal standard for NMR analysis.

## 2.3. Reactivity studies

### 2.3.1. Reaction of $[\{\text{IrCl}(\text{COD})\}_2]$ and $\text{Me}_2\text{SiHCl}$

NMR-scale: In an NMR tube equipped with a J. Young valve, 8.10 mg  $[\{\text{IrCl}(\text{COD})\}_2]$  (12.1  $\mu\text{mol}$ , 1.0 equiv.) is dissolved in 0.5 mL  $\text{CD}_2\text{Cl}_2$  and 21.4  $\mu\text{L}$   $\text{Me}_2\text{SiHCl}$  (18.3 mg, 193  $\mu\text{mol}$ , 16 equiv.) is added to the reaction mixture.  $\text{CHCl}_3$  is used as internal standard for NMR analysis.

TEM: 153 mg  $[\{\text{IrCl}(\text{COD})\}_2]$  (228  $\mu\text{mol}$ , 1.0 equiv.) is dissolved in 10 mL  $\text{CH}_2\text{Cl}_2$  and 401  $\mu\text{L}$   $\text{Me}_2\text{SiHCl}$  (345 mg, 3.65 mmol, 16 equiv.) are added to the reaction mixture. After stirring for 30 min at room temperature, the volatiles are removed at reduced pressure and the solid is dried at 200 °C for 5 h. For TEM analysis, the particles are suspended in ethanol.

UV–Vis: 2.45 mg  $[\{\text{IrCl}(\text{COD})\}_2]$  (3.65  $\mu\text{mol}$ , 1.0 equiv.) is dissolved in 23 mL  $\text{CH}_2\text{Cl}_2$  and 1.5 mL of the solution is transferred to a 1 cm UV–Vis cuvette for UV–Vis analysis. The solutions are combined and 6.42  $\mu\text{L}$   $\text{Me}_2\text{SiHCl}$  (5.52 mg, 58.3  $\mu\text{mol}$ , 16 equiv.) is added. Again, 1.5 mL of the solution is transferred to a 1 cm UV–Vis cuvette for UV–Vis analysis.

### 2.3.2. Reaction of $[\{\text{IrCl}(\text{COD})\}_2]$ and a mixture of $\text{Me}_2\text{SiHCl}/\text{MeSiHCl}_2$

In an NMR tube equipped with a J. Young valve, a mixture of 32.1  $\mu\text{L}$   $\text{Me}_2\text{SiHCl}$  (27.6 mg, 292  $\mu\text{mol}$ , 10 equiv.) and 30.5  $\mu\text{L}$   $\text{MeSiHCl}_2$  (33.6 mg, 292  $\mu\text{mol}$ , 10 equiv.) in 1.0 mL  $\text{CD}_2\text{Cl}_2$  is added to a solution of 19.6 mg  $[\{\text{IrCl}(\text{COD})\}_2]$  (29.2  $\mu\text{mol}$ , 1.0 equiv.) in 1.6 mL  $\text{CD}_2\text{Cl}_2$ .  $\text{CHCl}_3$  is used as internal standard for NMR analysis.

### 2.3.3. Synthesis of $[\text{Ir}(\text{allyl})(\text{Cl})_2(\text{COD})]$

1.11 g  $[\{\text{IrCl}(\text{COD})\}_2]$  (1.65 mmol, 1.0 equiv.) is dissolved in 20 mL  $\text{CH}_2\text{Cl}_2$ . 1.35 mL allyl chloride (1.26 g, 16.5 mmol, 10 equiv.) is added, the reaction mixture is stirred for 15 min at room temperature and all volatiles are removed in vacuum.  $[\text{Ir}(\text{allyl})(\text{Cl})_2(\text{COD})]$  is obtained in quantitative yield.  $^1\text{H}$  NMR (major isomer; 400 MHz,  $\text{CD}_2\text{Cl}_2$ , 213 K):  $\delta$  = 1.66 (m, 1 H,  $\text{CH}_2\text{-COD}$ ), 1.87 (m, 1 H,  $\text{CH}_2\text{-COD}$ ), 2.37–2.51 (m, 3 H,  $\text{CH}_2\text{-COD}$ ), 2.62–2.77 (m, 1 H,  $\text{CH}_2\text{-COD}$ ), 3.00 (dd,  $^2J_{\text{H,H}} = 15.4$  Hz,  $^3J_{\text{H,H}} = 8.2$  Hz, 1 H,  $\text{CH}_2\text{-COD}$ ), 3.22 (m, 1 H,  $\text{CH}_2\text{-COD}$ ), 3.42 (pseudo-q,  $^3J_{\text{H,H}} = 8.2$  Hz, 1 H, CH-COD), 3.49 (d,  $^3J_{\text{H,H}} = 13.9$  Hz, 1 H, *anti*  $\text{CH}_2\text{-allyl}$ ), 3.76 (d,  $^3J_{\text{H,H}} = 10.1$  Hz, 1 H, *anti*  $\text{CH}_2\text{-allyl}$ ), 4.32 (d,  $^3J_{\text{H,H}} = 7.2$  Hz, 1 H, *syn*  $\text{CH}_2\text{-allyl}$ ), 4.62 (pseudo-q,  $^3J_{\text{H,H}} = 8.2$  Hz, 1 H, CH-COD), 4.92 (pseudo-t,  $^3J_{\text{H,H}} = 7.3$  Hz, 1 H, CH-COD), 4.97 (d,  $^3J_{\text{H,H}} = 8.6$  Hz, 1 H, *syn*  $\text{CH}_2\text{-allyl}$ ), 5.07 (pseudo-t,  $^3J_{\text{H,H}} = 7.3$  Hz, 1 H, CH-COD), 5.67–5.77 (m, 1 H, CH-allyl).  $^{13}\text{C}$   $\{^1\text{H}\}$  NMR (major isomer; 101 MHz,  $\text{CD}_2\text{Cl}_2$ , 213 K):  $\delta$  [ppm] = 25.5 ( $\text{CH}_2\text{-COD}$ ), 28.4 ( $\text{CH}_2\text{-COD}$ ), 35.3 ( $\text{CH}_2\text{-COD}$ ), 36.8 ( $\text{CH}_2\text{-COD}$ ), 43.6 ( $\text{CH}_2\text{-allyl}$ ), 84.2 ( $\text{CH}_2\text{-allyl}$ ), 85.9 (CH-COD), 88.5 (CH-COD), 92.1 (CH-COD), 93.8 (CH-COD), 118.4 (CH-allyl).  $^1\text{H}$  NMR (minor isomer; 400 MHz,  $\text{CD}_2\text{Cl}_2$ , 213 K):  $\delta$  [ppm] = 1.26 (m, 1 H,  $\text{CH}_2\text{-COD}$ ), 1.66\* (1 H,  $\text{CH}_2\text{-COD}$ ), 2.18 (dd,  $^2J_{\text{H,H}} = 14.7$  Hz,  $^3J_{\text{H,H}} = 8.9$  Hz, 1 H,  $\text{CH}_2\text{-COD}$ ), 2.25–2.33 (m, 1 H,  $\text{CH}_2\text{-COD}$ ), 2.37–2.51\* (1 H,  $\text{CH}_2\text{-COD}$ ), 2.62–2.77\* (1 H,  $\text{CH}_2\text{-COD}$ ), 2.88 (dd,  $^2J_{\text{H,H}} = 15.6$  Hz,  $^3J_{\text{H,H}} = 8.0$  Hz, 1 H,  $\text{CH}_2\text{-COD}$ ), 2.97–3.03\* (1 H,  $\text{CH}_2\text{-COD}$ ), 4.24 (pseudo-q,  $^3J_{\text{H,H}} = 8.0$  Hz, 1 H, CH-COD), 4.31–4.34\* (1 H, *anti*  $\text{CH}_2\text{-allyl}$ ), 4.49 (d,  $^3J_{\text{H,H}} = 4.5$  Hz, 1 H, *syn*  $\text{CH}_2\text{-allyl}$ ), 4.59–4.65\* (1 H, CH-COD), 4.72 (m, 1 H, CH-COD), 5.05–5.09\* (2 H, CH-allyl, *anti*  $\text{CH}_2\text{-allyl}$ ), 5.17 (d,  $^3J_{\text{H,H}} = 4.5$  Hz, 1 H, *syn*  $\text{CH}_2\text{-allyl}$ ), 5.54 (dd,  $^3J_{\text{H,H}} = 6.0$  Hz,  $^3J_{\text{H,H}} = 8.0$  Hz, 1 H, CH-COD).  $^{13}\text{C}$   $\{^1\text{H}\}$  NMR (minor isomer; 101 MHz,  $\text{CD}_2\text{Cl}_2$ , 213 K):  $\delta$  [ppm] = 25.9 ( $\text{CH}_2\text{-COD}$ ), 28.4 ( $\text{CH}_2\text{-COD}$ ), 34.0 ( $\text{CH}_2\text{-COD}$ ), 37.3 ( $\text{CH}_2\text{-COD}$ ), 45.3 ( $\text{CH}_2\text{-allyl}$ ), 86.2 (CH-COD), 87.1 (CH-COD), 88.1 (CH-COD), 93.3 (CH-COD), 94.8 ( $\text{CH}_2\text{-allyl}$ ), 110.4 (CH-allyl). MS (FAB):  $m/z$  (%) = 713 (51)  $[\text{M} - \text{allyl} - 2\text{Cl}]^+$ , 377 (51)  $[\text{M} - \text{Cl}]^+$ , 335 (100)  $[\text{M} - \text{allyl} - \text{Cl} - \text{H}]^+$ . Elemental analysis (%): calc.: C, 32.04; H, 4.16. found: C, 31.82; H, 4.25. \*Overlapping signals with major isomer.

### 2.3.4. Reaction of $[\text{Ir}(\text{allyl})(\text{Cl})_2(\text{COD})]$ and $\text{Me}_2\text{SiHCl}$

In an NMR tube equipped with a J. Young valve, 22.2 mg  $[\text{Ir}(\text{allyl})(\text{Cl})_2(\text{COD})]$  (53.8  $\mu\text{mol}$ , 1.0 equiv.) is dissolved in 1.6 mL  $\text{CD}_2\text{Cl}_2$  and 47.4  $\mu\text{L}$   $\text{Me}_2\text{SiHCl}$  (40.8 mg, 431  $\mu\text{mol}$ , 8.0 equiv.) in 1.0 mL  $\text{CD}_2\text{Cl}_2$  is added to the reaction mixture.  $\text{CHCl}_3$  is used as internal standard for NMR analysis.

## 3. Results and discussion

### 3.1. Influence of catalyst/co-catalyst concentration and the rate of silane addition on catalytic performance

The commonly used model system in iridium-catalyzed hydrosilylation of allyl compounds is the reaction of allyl chloride and  $\text{Me}_2\text{SiHCl}$ , with  $[\{\text{IrCl}(\text{COD})\}_2]$  and cyclooctadiene (COD) as catalyst/co-catalyst combination, to yield chloro(3-chloropropyl) dimethylsilane (Scheme 2) [11–22].

Typically, the silane (1.0 equiv.) is slowly added to a mixture of the allyl compound (1.0 equiv.), the catalyst and the co-catalyst at 40 °C under neat conditions. Interestingly, three parameters differ



**Scheme 2.** Hydrosilylation of allyl chloride and  $\text{Me}_2\text{SiHCl}$  to yield chloro(3-chloropropyl)dimethylsilane [11–22].

significantly in the experimental sections of the patent reports [11–22]:

1. Catalyst concentration: 40–360 ppm.
2. Co-catalyst concentration: 80–2300 ppm.
3. Rate of silane addition: 0.0028–0.011 equiv.  $\text{min}^{-1}$ .

In order to better understand this model system, it appeared to be necessary to reproduce the results from patent literature and then elucidate the influence of the abovementioned parameters on the catalytic performance. In a typical catalytic experiment,  $[\text{IrCl(COD)}]_2$ , COD and allyl chloride were stirred for 10 min at 40 °C, before  $\text{Me}_2\text{SiHCl}$  was added over a defined period of time. When the addition was completed, mesitylene was added as internal standard and after further 10 min, an aliquot was taken for NMR analysis.

The first parameter of interest was the catalyst concentration, i.e. the employed amount of  $[\text{IrCl(COD)}]_2$ . With differing iridium concentrations at a constant COD concentration (10,000 ppm) as well as a fixed rate of  $\text{Me}_2\text{SiHCl}$  addition (0.061 equiv.  $\text{min}^{-1}$ , 200 mmol/h), the yield of the obtained  $\gamma$ -substituted propylsilane was determined and the results are shown in Fig. 1.

While low amounts of iridium up to 20 ppm do not result in significant product formation (3% yield), a considerable increase can be observed at 40 ppm (20% yield) with an overall sigmoidal progression up to 80 ppm with quantitative product yield. This indicates substantial catalyst deactivation at low iridium concentrations in the reaction mixture, which might point toward a dependence on the employed iridium to silane ratio. Another reason might be impurities in the mixture, which deactivate a certain amount of the catalyst leading to low yields at small iridium

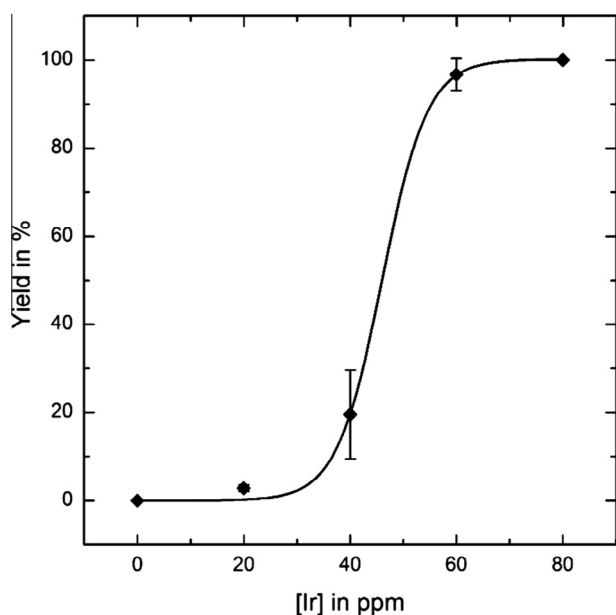


**Fig. 1.** Average yield of chloro(3-chloropropyl)dimethylsilane as a function of the iridium concentration; COD concentration of 10,000 ppm and rate of  $\text{Me}_2\text{SiHCl}$  addition at 0.061 equiv.  $\text{min}^{-1}$ ; at least three catalytic runs per data point with the standard deviation as  $\pm y$  error bars ( $R^2 = 0.999$ ).

loadings and the quite substantial yield increase starting around 40 ppm. The results do not depend on the reaction time, i.e. if the reaction mixture is further stirred at 40 °C after silane addition and aliquots for analysis are taken every hour, the yields remain unaltered.

The rate of silane addition was the influence factor studied next, with an iridium concentration of 20 ppm and 10,000 ppm of COD (Fig. 2).

With an increasing rate of silane addition, the yields of the desired hydrosilylation product drop drastically, in an inverse exponential fashion. This strengthens the assumed relationship between silane concentration and deactivation, with the latter being caused by a local “overconcentration” of silane in solution. The average values for the yields range from over 60% yield at 0.0038 equiv.  $\text{min}^{-1}$  to under 2% at 0.12 equiv.  $\text{min}^{-1}$ . It seems worth noting that the standard deviations at very slow addition rates are quite substantial. One reason might be the fact that these data points are within the steepest regime of the curve, possibly leading to relatively large differences in yield caused by even small perturbations in the reaction setup. Within all experiments carried out in this study, these are by far the most significant fluctuations. When the average yield of chloro(3-chloropropyl)dimethylsilane is plotted against the iridium concentration over the rate of silane addition, the graph implies a linear relation (see [Supplementary Material](#)). This again shows the importance of the iridium to silane ratio.

Finally, the influence of the amount of COD was studied. The iridium concentration was again kept at 20 ppm, with a silane addition rate of 0.015 equiv.  $\text{min}^{-1}$  (50 mmol/h). Since the reported COD concentrations in patent literature vary strongly, the employed co-catalyst concentrations range over six orders of magnitude and are shown in Fig. 3 with a logarithmic x-axis.

The overall curve shows a sigmoidal progression with the first significant product yield increase at 10,000 ppm of COD (17% yield), while up to 1,000 ppm, the yields are comparably low at 3–5%. A further increase to 25% yield can be achieved at  $[\text{COD}] = 100,000$  ppm; however, this seems unreasonable from an

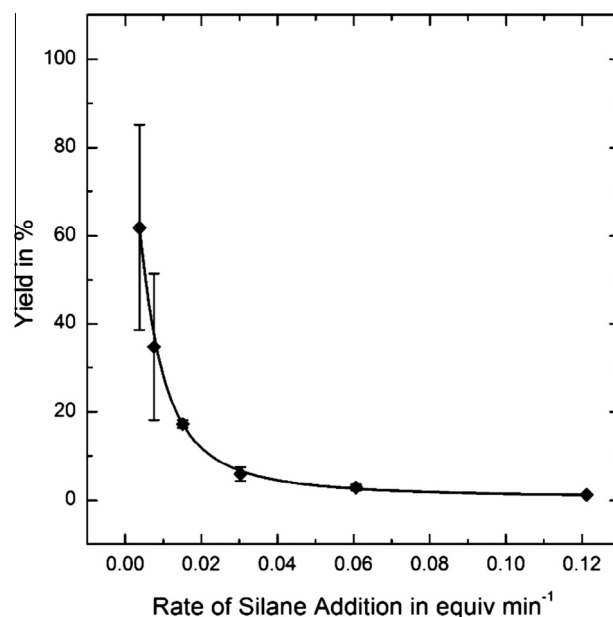


**Fig. 2.** Average yield of chloro(3-chloropropyl)dimethylsilane as a function of the rate of silane addition; iridium concentration of 20 ppm and COD concentration of 10,000 ppm; at least three catalytic runs per data point with the standard deviation as  $\pm y$  error bars ( $R^2 = 0.997$ ).

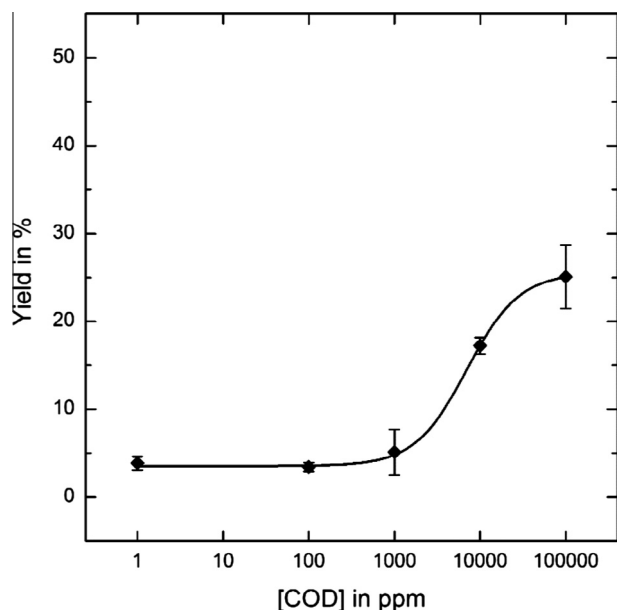


**Fig. 3.** Average yield of chloro(3-chloropropyl)dimethylsilane as a function of the COD concentration: iridium concentration of 20 ppm and rate of  $\text{Me}_2\text{SiHCl}$  addition at  $0.015 \text{ equiv. min}^{-1}$ ; 100 ppm of COD was the first concentration which could be experimentally realized, and the value at 1 ppm correlates to  $[\text{COD}] = 0 \text{ ppm}$ ; at least three catalytic runs per data point with the standard deviation as  $\pm$  error bars ( $R^2 = 0.995$ ).

experimental point of view, considering that the co-catalyst then amounts to over 9% of the total reaction volume.

In summary, all three parameters investigated influence the yield of chloro(3-chloropropyl)dimethylsilane significantly. It can be concluded that the yield can be improved by the following:

1. Increased catalyst loadings.
2. Higher concentration of co-catalyst.
3. Decreased rate of silane addition.

(In cases 1 and 2 an optimum concentration can be found. With an elevation beyond that value no further increase in yield takes place.)

### 3.2. Reactions of the iridium precursor and the substrates

After investigating the main parameters influencing the catalytic performance, further reactivity studies were conducted. A reaction of  $[\{\text{IrCl}(\text{COD})\}_2]$  and  $\text{Me}_2\text{SiHCl}$  (16 equiv.) was used to elucidate the main catalyst deactivation pathway at high silane concentrations (Scheme 3).

The reaction of  $[\{\text{IrCl}(\text{COD})\}_2]$  and  $\text{Me}_2\text{SiHCl}$  yields about 90% of cyclooctane in a formal hydrogenation reaction, iridium nanoparticles and a mixture of different chloromethylsilanes, formed by halide abstraction and  $\text{Si-R/-X}$  redistribution [26,27]. The ability of the chlorinated silane to reduce the metal center and the olefin ligand appears interesting, since it has been reported for reactions with alkylhydrosilanes that the olefin ligands on halide-bridged iridium complexes simply decoordinate and the metal stays in its oxidation state [26–28]. In these reports, both the olefin and the halide ligands are replaced by silyl and bridging silylene ligands,

respectively. This experiment illustrates that the increased polarity via chlorination of the silane significantly increases its ability to reduce ligand and metal, leading to decomposition of the catalyst as soon as the iridium to silane ratio is too small, i.e. either small amounts of catalyst are present or the silane addition rate is high.

A combination of TEM and UV–Vis measurements was used to verify the formation of iridium nanoparticles (Figs. 4 and 5). These are common techniques in the characterization of iridium particles, which are usually obtained from reactions of various iridium precursors and dihydrogen [29–32].

The iridium nanoparticles for TEM analysis were obtained from the reaction solution by evaporation of all volatile compounds at high temperature. For UV–Vis measurements, a spectrum of  $[\{\text{IrCl}(\text{COD})\}_2]$  was recorded and further monitored over time after addition of  $\text{Me}_2\text{SiHCl}$ . The absorption bands between 300 and 500 nm instantaneously disappear and only one strong band at 240 nm remains, which is characteristic for iridium nanoparticles [31,32].

The formation of particles queried whether the process is homogeneously or heterogeneously catalyzed; thus, the iridium nanoparticles were employed in catalysis. From now on, the following conditions were used for the catalytic experiments: iridium concentration of 100 ppm, COD concentration of 10,000 ppm and a rate of silane addition at  $0.061 \text{ equiv. min}^{-1}$  (200 mmol/h). As shown in Fig. 5, particles form immediately after  $[\{\text{IrCl}(\text{COD})\}_2]$  is exposed to  $\text{Me}_2\text{SiHCl}$ . Therefore, an “inverse” reaction protocol was used to evaluate whether the iridium nanoparticles are active in catalysis.  $[\{\text{IrCl}(\text{COD})\}_2]$ , COD and  $\text{Me}_2\text{SiHCl}$  were mixed and allyl chloride was slowly added over time, i.e. the addition of the substrates was inverted. With this procedure, the desired chloro(3-chloropropyl)dimethylsilane is obtained in slightly over 1% yield, while the blind reaction without iridium does not yield any product and the “normal” reaction protocol with the slow addition

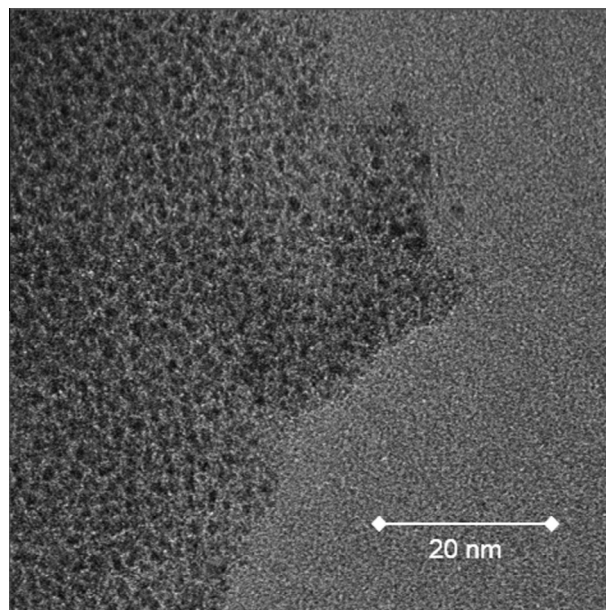
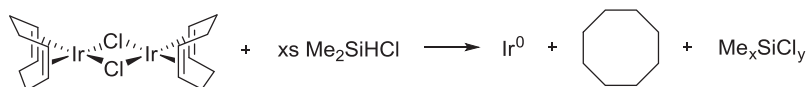


**Fig. 4.** TEM image of iridium nanoparticles isolated from a reaction of  $[\{\text{IrCl}(\text{COD})\}_2]$  and  $\text{Me}_2\text{SiHCl}$ .



**Scheme 3.** Reaction of  $[\{\text{IrCl}(\text{COD})\}_2]$  and  $\text{Me}_2\text{SiHCl}$ .



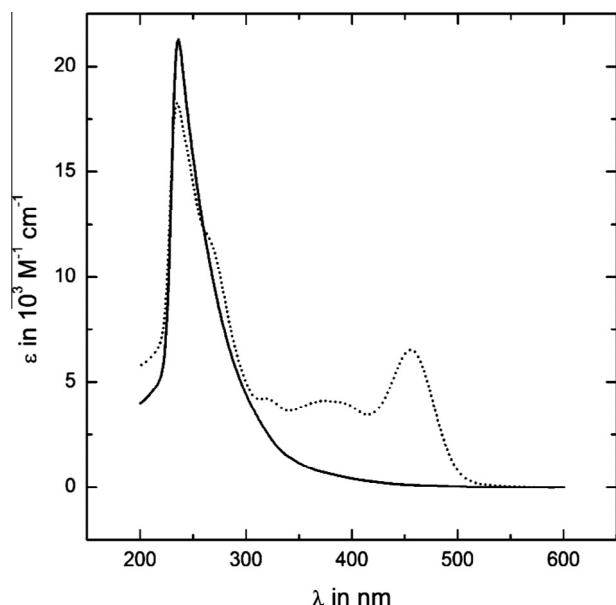


**Fig. 5.** UV-Vis spectra of  $[\{\text{IrCl}(\text{COD})\}_2]$  (dotted line) and the formation of iridium nanoparticles (solid line, first spectrum measured 3 min after silane addition) upon reaction with  $\text{Me}_2\text{SiHCl}$ .

of silane to an iridium/COD/allyl compound mixture yields the product in >99%. These results, in combination with the yield dependence on the rate of silane addition support the assumption that the reaction is mostly homogeneously catalyzed and the contribution from the formed iridium nanoparticles is very minor at best.

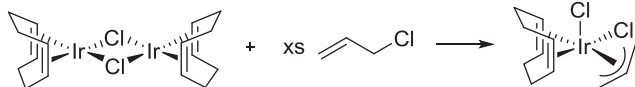
After stoichiometric reactions with the silane, the catalyst precursor  $[\{\text{IrCl}(\text{COD})\}_2]$  was treated with excess allyl chloride (10 equiv.; [Scheme 4](#)).

The iridium dimer is opened by oxidative addition, resulting in quantitative formation of the respective allyl iridium(III) compound. This is interesting due to reports on dimer opening by simple coordination of the double bond rather than via C–Cl activation [1,33]. However, it does not seem surprising since similar reactivities have been observed for reactions with allyl bromo/chloro derivatives [34,35]. With regard to  $^1\text{H}$  NMR spectroscopy, the signals of  $[\text{Ir}(\text{allyl})(\text{Cl})_2(\text{COD})]$  at room temperature in  $\text{CD}_2\text{Cl}_2$  are particularly broad but measurements at  $-60^\circ\text{C}$  reveal a very defined spectrum and in combination with 2D NMR experiments, two isomers in a ratio of 10:3 (different orientation of the allyl ligand) can be identified ([Fig. 6](#) and [Supplementary Material](#)).

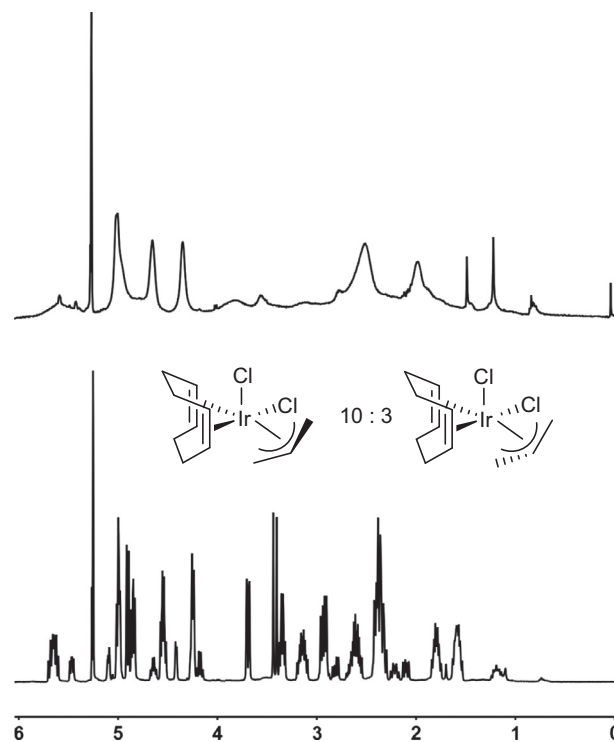
### 3.3. Expansion of the substrate scope

In order to understand the capabilities and limitations of the iridium-catalyzed hydrosilylation of allyl compounds compared to the platinum-based systems, the substrate scope was expanded toward the higher chlorinated silane  $\text{MeSiHCl}_2$  and allyl ethyl ether as the olefin ([Table 1](#)).

While the hydrosilylation of allyl chloride and  $\text{Me}_2\text{SiHCl}$  gives the desired  $\gamma$ -substituted product in quantitative yield, the use of



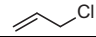
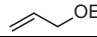
**Scheme 4.** Reaction of  $[\{\text{IrCl}(\text{COD})\}_2]$  and allyl chloride.



**Fig. 6.**  $^1\text{H}$  NMR spectra of  $[\text{Ir}(\text{allyl})(\text{Cl})_2(\text{COD})]$  in  $\text{CD}_2\text{Cl}_2$  at room temperature (top) and at  $-60^\circ\text{C}$  (bottom, x-axis in ppm), two isomers with ratio at  $-60^\circ\text{C}$  in  $\text{CD}_2\text{Cl}_2$  depicted in the middle.

**Table 1**

Yield of  $\gamma$ -substituted product in the iridium-catalyzed hydrosilylation of allyl compounds; iridium concentration: 100 ppm, COD concentration: 10,000 ppm, rate of silane addition:  $0.061 \text{ equiv. min}^{-1}$ .

		
$\text{Me}_2\text{SiHCl}$	>99%	75%
$\text{MeSiHCl}_2$	3%	3%

allyl ethyl ether only results in 75% product formation. Compared to allyl chloride (>99% selectivity), the selectivity is lower (85%). About 12% of allyl ethyl ether are not converted, while the main by-products are cis- and trans-isomerized starting material – i.e. after double bond isomerization to the internal position adjacent to the ether oxygen atom – with 7% and 2%, respectively. Similar iridium-catalyzed isomerization processes have been reported [23,36]. Since internal olefins are more difficult to be transformed in catalytic hydrosilylation [3], this might be the reason for the lower product yield and selectivity, as the olefin then occupies a coordination site on the metal without reacting with the silane; thus, the silane can possibly deactivate the catalyst.

When the higher homologue  $\text{MeSiHCl}_2$  was employed as substrate, only 3% of the respective dichloromethylsilanes are obtained for both allyl chloride and allyl ethyl ether. Therefore, in analogy to the reaction illustrated in [Scheme 3](#),  $[\{\text{IrCl}(\text{COD})\}_2]$  was exposed to an excess of an equimolar mixture of  $\text{Me}_2\text{SiHCl}/\text{MeSiHCl}_2$  (10 equiv. each). Again, cyclooctane, iridium nanoparticles and different chloromethylsilanes are yielded; however, the consumption of  $\text{MeSiHCl}_2$  exceeds the one of  $\text{Me}_2\text{SiHCl}$  by a factor of 1.4. This implies that a higher degree of chlorination facilitates the reaction of the catalyst to the deactivation products, which is in accord with the observations for the platinum-catalyzed variant [4]. Oxidative addition of an increasingly electron-deficient silane – i.e. higher degree of chlorination – to the olefin-bound,

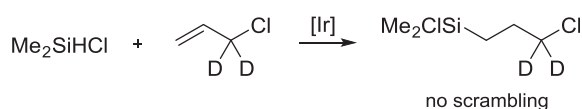
electron-poor metal results in an extremely electron-deficient metal species, which is prone to decomposition processes.

### 3.4. Mechanistic aspects

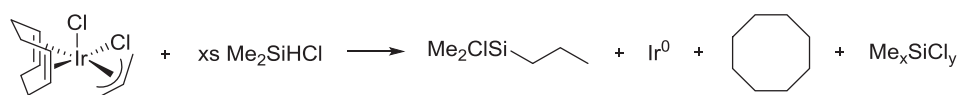
To obtain a profound mechanistic picture for the iridium-catalyzed hydrosilylation of allyl compounds, further experiments were performed. In a stoichiometric experiment analogous to the reaction shown in Scheme 4,  $[\text{IrCl}(\text{COD})]_2$  was treated with an excess of allyl ethyl ether. However, no reaction occurs and the dimeric iridium structure stays intact as indicated by  $^1\text{H}$  NMR spectroscopy. This is distinctly different to the reactivity with allyl chloride, which quantitatively yields  $[\text{Ir}(\text{allyl})(\text{Cl})_2(\text{COD})]$  (vide supra).

Due to this fact, it appeared interesting whether or not the two substrates are transformed in mechanistically different catalytic cycles or what the role of the allyl intermediate really is. Therefore, deuterated allyl chloride was employed in a catalytic run with  $\text{Me}_2\text{SiHCl}$  (Scheme 5).

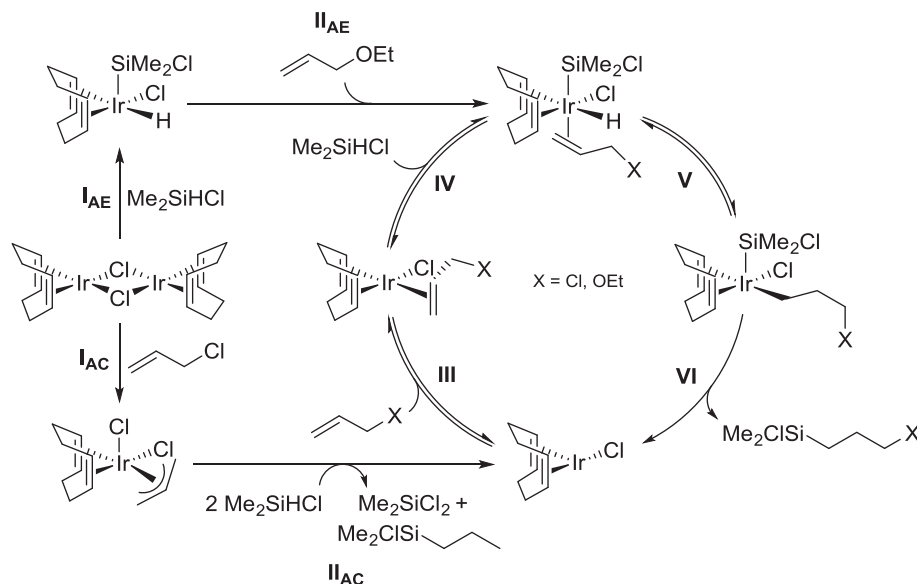
The reaction does not result in any scrambling/shift of the deuterated methylene group which seems surprising, given the fact that  $[\text{Ir}(\text{allyl})(\text{Cl})_2(\text{COD})]$  is quantitatively formed after exposure to allyl chloride (Scheme 4). Therefore, no allyl intermediate is part of the catalytic cycle since allyl formation would lead to a full scrambling of the  $\text{d}_2$ -group in the product. To further understand whether the allyl ligand can in general lead to product formation, isolated  $[\text{Ir}(\text{allyl})(\text{Cl})_2(\text{COD})]$  was treated with an excess of  $\text{Me}_2\text{SiHCl}$  (8.0 equiv.; Scheme 6).



Scheme 5. Catalytic run with allyl chloride- $\text{d}_2$  and  $\text{Me}_2\text{SiHCl}$ .



Scheme 6. Reaction of  $[\text{Ir}(\text{allyl})(\text{Cl})_2(\text{COD})]$  and  $\text{Me}_2\text{SiHCl}$ .



Scheme 7. Proposed mechanistic picture for the iridium-catalyzed hydrosilylation of allyl compounds.

No chloro(3-chloropropyl)dimethylsilane is obtained, but instead the linear/defunctionalized propylsilane is formed in quantitative yield as well as the typical deactivation products. These two findings (Schemes 5 and 6) prove that neither  $[\text{Ir}(\text{allyl})(\text{Cl})_2(\text{COD})]$  nor any allyl intermediate are part of the catalytic cycle itself and no product is formed from the allyl complex.

For the hydrosilylation of allyl ethyl ether, it appeared worthwhile studying the importance of dimer opening of the catalyst precursor  $[\{\text{IrCl}(\text{COD})\}_2]$ . Since allyl ethyl ether is not able to open the iridium dimer,  $[\text{Ir}(\text{allyl})(\text{Cl})_2(\text{COD})]$  was employed as catalyst precursor in a reaction of allyl ethyl ether and  $\text{Me}_2\text{SiHCl}$ . Almost no difference in catalytic performance is observed with regard to the employed iridium source, which suggests that  $\text{Me}_2\text{SiHCl}$  is also able to open the dimeric compound by oxidative addition and enables catalysis. Since the reaction is performed neatly in the allyl compound and the silane is just added slowly, the “silane-opened” iridium dimer is immediately coordinated by the alkene. No additional deactivation through formal ligand hydrogenation and iridium particle formation occurs as compared to starting from  $[\text{Ir}(\text{allyl})(\text{Cl})_2(\text{COD})]$ .

By combining the obtained data, the following mechanistic picture for the iridium-catalyzed hydrosilylation of allyl compounds is proposed (Scheme 7).

In the catalytic hydrosilylation of allyl chloride starting from  $[\{\text{IrCl}(\text{COD})\}_2]$ , the first step is the quantitative conversion of the iridium dimer to  $[\text{Ir}(\text{allyl})(\text{Cl})_2(\text{COD})]$  ( $\text{I}_{\text{AC}}$ ), which is followed by cleavage of the allyl ligand with two equivalents of  $\text{Me}_2\text{SiHCl}$  to form  $\text{Me}_2\text{SiCl}^n\text{Pr}$  and  $\text{Me}_2\text{SiCl}_2$  ( $\text{II}_{\text{AC}}$ ). The resulting  $[\text{IrCl}(\text{COD})]$  is coordinated by the olefin ( $\text{III}$ ) and oxidative addition of the silane ( $\text{IV}$ ) yields an iridium(III) intermediate. The coordinated alkene is converted to an alkyl ligand upon hydride transfer ( $\text{V}$ ) which ultimately yields the product after reductive elimination ( $\text{VI}$ ) and regenerates the catalyst in its resting state ( $[\text{IrCl}(\text{COD})]$ ). For allyl ethyl ether as substrate, only the first two reaction steps are different: The iridium dimer is opened via oxidative addition of the

silane (**I<sub>AE</sub>**) and subsequent coordination of the alkene (**II<sub>AE</sub>**) is necessary to enter the catalytic cycle.

When the local silane concentration during catalysis becomes too high, i.e. the iridium to silane ratio is too low, the respective iridium intermediates are prone to leaving the catalytic cycle upon reacting to iridium nanoparticles and cyclooctane. Exemplarily, when [IrCl(COD)] reacts with silane, the silyl hydrido complex [IrClH(SiMe<sub>2</sub>Cl)(COD)] is formed, which is known to be an intermediate in the catalyst deactivation pathway (Scheme 3). This deactivation can be prevented by application of an excess of COD (Fig. 3). This is most probably caused by coordination and replacement of partially hydrogenated ligand, keeping the active catalyst in solution.

#### 4. Conclusion

For the first time a comprehensive mechanistic understanding of the iridium-catalyzed hydrosilylation of allyl compounds can be presented. To achieve this, a combination of stoichiometric and catalytic experiments has been used. The main reason for the short catalyst lifetimes is found to be the formal hydrogenation of the cyclooctadiene (COD) ligands on [IrCl(COD)]<sub>2</sub> and the formation of iridium nanoparticles at elevated silane concentrations. Possible solutions regarding the reaction setup are a slower rate of silane addition and an increased concentration of cyclooctadiene in the short term. For further fundamental improvements, we are currently synthesizing and employing new catalyst motifs which should pave the way toward a more generally applicable iridium-catalyzed hydrosilylation of allyl compounds; especially focusing on allyl chloride, the most widely used allyl compound in industry. Since there are reports on iridium complexes bearing olefin ligands which are not prone to hydrogenation, the concept is to mimic the electronic structure of [IrCl(COD)]<sub>2</sub> while preventing deactivation via formal hydrogenation, i.e. hydrogen transfer from R<sub>3</sub>Si–H to the alkene. Ultimately, the combination of iridium- and platinum-catalyzed processes in the hydrosilylation of allyl compounds will be complementary for a broad range of substrates. While the latter process is fairly established for allyl acetate, ethers and amines, iridium-catalysis is superior in the hydrosilylation of allyl chloride due to the intrinsic selectivity issues of platinum catalysis.

#### Acknowledgments

Support from the Fonds der Chemischen Industrie (Ph.D. grants to T.K.M. and K.R.) and the TUM Graduate School is gratefully acknowledged. Further, we thank Dr. Jürgen Stohrer for helpful discussions.

#### Appendix A. Supplementary material

Supplementary data associated with this article can be found, in the online version, at <http://dx.doi.org/10.1016/j.jcat.2015.09.003>.

#### References

- [1] D. Troegel, J. Stohrer, *Coord. Chem. Rev.* 255 (2011) 1440–1459.
- [2] Y. Nakajima, S. Shimada, *RSC Adv.* 5 (2015) 20603–20616.
- [3] B. Marciniak, *Hydrosilylation: A Comprehensive Review on Recent Advances*, Springer, London, 2008.
- [4] P. Gigler, M. Drees, K. Riener, B. Bechlers, W.A. Herrmann, F.E. Kühn, *J. Catal.* 295 (2012) 1–14.
- [5] B. Marciniak, H. Maciejewski, W. Duczmal, R. Fiedorow, D. Kityński, *Appl. Organomet. Chem.* 17 (2003) 127–134.
- [6] M. Jankowiak, H. Maciejewski, J. Gulinski, *J. Organomet. Chem.* 690 (2005) 4478–4487.
- [7] Z.V. Belyakova, E.A. Chernyshev, P.A. Storozhenko, S.P. Knyazev, G.N. Turkel'taub, E.V. Parshina, A.V. Kisin, *Russ. J. Gen. Chem.* 76 (2006) 925–930.
- [8] A. Wawrzyńczak, M. Dutkiewicz, J. Guliński, H. Maciejewski, B. Marciniak, R. Fiedorow, *Catal. Today* 169 (2011) 69–74.
- [9] M. Igarashi, T. Kobayashi, K. Sato, W. Ando, T. Matsumoto, S. Shimada, M. Hara, H. Uchida, *J. Organomet. Chem.* 725 (2013) 54–59.
- [10] M. Igarashi, T. Matsumoto, T. Kobayashi, K. Sato, W. Ando, S. Shimada, M. Hara, H. Uchida, *J. Organomet. Chem.* 749 (2014) 421–427.
- [11] A. Bauer, O. Schäfer, M. Kriegbaum, L. Brader, B. Pachaly, V. Frey, US6388119, 2002 (to Consortium für elektrochemische Industrie GmbH).
- [12] Y. Tonomura, T. Kubota, M. Endo, US6359161, 2002 (to Shin-Etsu Chemical Co., Ltd.).
- [13] A. Bauer, L. Brader, V. Frey, M. Kriegbaum, B. Pachaly, O. Schäfer, EP1201671B1, 2003 (to Consortium für elektrochemische Industrie GmbH).
- [14] F. Baumann, M. Hoffmann, DE10200405242A1, 2006 (to Wacker Chemie AG).
- [15] Y. Tonomura, T. Kubota, M. Endo, EP1156052B1, 2006 (to Shin-Etsu Chemical Co., Ltd.).
- [16] F. Baumann, DE102005030581A1, 2007 (to Wacker Chemie AG).
- [17] T. Kornek, A. Bauer, D. Senden, US7208618, 2007 (to Wacker Chemie AG).
- [18] K. Ramdani, B. Vogin, N. Guennouni, EP1515977B1, 2007 (to Rhodia Chimie SA).
- [19] K. Ramdani, N. Guennouni, B. Vogin, EP1637534B1, 2009 (to Rhodia Chimie).
- [20] K. Ramdani, B. Vogin, N. Guennouni, US7655813, 2010 (to Rhodia Chimie).
- [21] K. Ramdani, B. Vogin, N. Guennouni, US7659418, 2010 (to Rhodia Operations).
- [22] N. Guennouni, J.-C. Galland, US7884225, 2011 (to Rhodia Chimie).
- [23] M. Igarashi, T. Matsumoto, T. Kobayashi, K. Sato, W. Ando, S. Shimada, M. Hara, H. Uchida, *J. Organomet. Chem.* 752 (2014) 141–146.
- [24] W.L.F. Armarego, C.L.L. Chai, *Purification of Laboratory Chemicals*, Butterworth-Heinemann, Oxford, 2013.
- [25] G.R. Fulmer, A.J.M. Miller, N.H. Sherden, H.E. Gottlieb, A. Nudelman, B.M. Stoltz, J.E. Bercaw, K.I. Goldberg, *Organometallics* 29 (2010) 2176–2179.
- [26] C. Cheng, M. Brookhart, *J. Am. Chem. Soc.* 134 (2012) 11304–11307.
- [27] S. Park, B.G. Kim, I. Göttker-Schnetmann, M. Brookhart, *ACS Catal.* 2 (2012) 307–316.
- [28] C. Cheng, M. Brookhart, *Angew. Chem. Int. Ed.* 51 (2012) 9422–9424.
- [29] J. Dupont, G.S. Fonseca, A.P. Umpierre, P.F.P. Fichtner, S.R. Teixeira, *J. Am. Chem. Soc.* 124 (2002) 4228–4229.
- [30] G.S. Fonseca, A.P. Umpierre, P.F.P. Fichtner, S.R. Teixeira, J. Dupont, *Chem.-Eur. J.* 9 (2003) 3263–3269.
- [31] V. Mévellec, A. Roucoux, E. Ramirez, K. Philippot, B. Chaudret, *Adv. Synth. Catal.* 346 (2004) 72–76.
- [32] R. Redón, F. Ramírez-Crescencio, A.L. Fernández-Osorio, *J. Nanopart. Res.* 13 (2011) 5959–5965.
- [33] G. Pannetier, P. Fougeroux, R. Bonnaire, *J. Organomet. Chem.* 38 (1972) 421–425.
- [34] B. Bartels, C. García-Yebra, F. Rominger, G. Helmchen, *Eur. J. Inorg. Chem.* 2002 (2002) 2569–2586.
- [35] C. García-Yebra, J.P. Janssen, F. Rominger, G. Helmchen, *Organometallics* 23 (2004) 5459–5470.
- [36] T. Ohmura, Y. Yamamoto, N. Miyaura, *Organometallics* 18 (1998) 413–416.